Seventh International Conference on CFD in the Minerals and Process Industries
CSIRO, Melbourne, Australia
9-11 December 2009

IMPLEMENTATION OF AN IMMERSED BOUNDARY METHOD IN SPECTRAL-ELEMENT SOFTWARE

Daniel R HILLIER[1], Kris RYAN[1] and Gregory J SHEARD[1]

[1] Fluids Laboratory for Aeronautical and Industrial Research (FLAIR), Department of Mechanical and Aerospace Engineering, Monash University, VIC 3800, AUSTRALIA

ABSTRACT

Implementation of moving and deforming boundaries within fluid solvers presents possibilities for the numerical analysis of fluid-structure interactions. This could lead to the optimization of many industrial phenomena, such as heat exchangers, tethered cylinders or many other applications where a moving body is present within a fluid. This paper focuses on the implementation of a numerical algorithm which will allow the simulation of moving boundaries and coupled fluid-solid interactions within a spectral element solver. To achieve this, a technique for the representation of a boundary in a fluid simulation that does not align with the computational grid, an immersed boundary method, has been applied. This allows the body the freedom to move without violating or requiring the adjustment of a traditional mesh. Details of the integration of the immersed boundary technique into a spectral-element fluid solver, which uses a backwards multistep method to evolve the solutions in time, is discussed. A two-dimensional test case, considering a cylinder in a cross flow which does not coincide with the mesh, was compared to a body fitted technique to ascertain the validity of the imposition of the immersed boundary condition of the current implementation. The technique produced good results, predicting the recirculation length behind the cylinder to 4.30% and 3.72% for the steady cases of $Re = 25$ and 30 respectively. Similarly, the prediction of the Strouhal numbers for the time-dependent cases of $Re = 100 – 200$ was computed to be within 2.2% of the body fitted case.

NOMENCLATURE

D	diameter of cylinder
p	pressure
f	shedding frequency
f_{IB}	pseudo forcing term
H	convective and viscous terms of the Navier-Stokes equations
h	characteristic length
$\mathbf{N}(\boldsymbol{u})$	non-linear operator
N	nodes per element
n	current timestep index
Re	Reynolds number
St	Strouhal number
T	shedding period
t	time
U	freestream velocity
$\mathbf{u}$	velocity vector
u_{virt}	velocity interpolated at a virtual point
u^*	velocity imposed on forcing point
$\hat{\mathbf{u}}$	intermediate velocity vector
$\hat{\hat{\mathbf{u}}}$	intermediate velocity vector
V_ψ	velocity on immersed boundary
$\mathbf{x}$	spatial vector
α	integration coefficient
β	integration coefficient
γ	integration coefficient
ρ	density
ν	kinematic viscosity

INTRODUCTION

Moving and deforming boundaries, a phenomenon where the bounding walls of the flow or an object in the flow deform or move, are a common occurrence in many engineering applications. The effects such interactions have on the flow can be significant and can dominate the subsequent flow, such as in the case of a marine riser pipe.

The numerical complexities of implementing a fluid-structure solver first arise when one considers the difficult process of moving a body on a computational domain. Most numerical methods use boundary conforming techniques, techniques in which the computational mesh is aligned with the boundaries defining the geometry the fluid flows through. There have been several adaptations of these methodologies to accommodate moving boundaries. An example of these adaptations is the coordinate transformations conducted by Newman and Karniadakis (1997). These methods, in general, only allow for particular geometries and only a single moving body. For complex geometries, including multiple bodies, it is necessary to deform or regenerate the computational mesh at every timestep to accommodate the boundaries moving relative to each other, decreasing the accuracy and efficiency of the fluid solvers (Yang *et al.* 2008).

Non-boundary conforming techniques, in which the boundaries and grid points do not necessarily coincide, are able to solve complex geometries and moving boundary scenarios on arbitrary meshes. This allows the solutions to be computed without the need for complicated, inaccurate and computationally expensive mesh regeneration. Unfortunately this convenience comes at a cost. By not having the boundaries coincide with the grid points, the boundary conditions are not easily enforced. An additional system is required to rectify this deficiency, which introduces some additional complexity and computational overhead to the underlying numerical scheme.

In the case of immersed boundary algorithms, this complexity is addressed through an additional forcing term in the governing equations. This term imposes the presence of the boundary upon selected points in the computational mesh which are in close proximity to the immersed boundary. This has been shown to provide a good representation of the boundary while being easily adapted into current finite difference and finite volume numerical solvers with little additional overhead (Balaras, 2004).

The current paper focuses on adapting a non-boundary conforming, immersed boundary algorithm to an in-house spectral-element solver (Sheard *et al*., 2007). The immersed boundary scheme considered here is derived from the scheme developed in Balaras (2004) which has been extended to accommodate moving boundaries and fluid-structure interactions as detailed in Yang *et al.* (2008). In particular, this paper focuses on discerning the viability of implementing the non-boundary conforming method, and the subsequent moving boundary method, into a spectral-element fluid solver. This was assessed through validating the case of a two-dimensional flow over a circular cylinder.

METHODOLOGY

The process of imposing the presence of an immersed boundary within a numerical flow solver can be split into two stages: the identification of forcing nodes and the application of a forcing term at these points.

Identification of Forcing Points

For a node to be identified as a forcing point, it must lie in the solid phase and have at least one neighbouring point in the fluid phase, as performed in Kim *et al.* (2001). Clearly, to achieve this, it is necessary to have detailed information about the boundary, be able to locate points which lie near the interface and be able to determine in which phase the node resides in. Accordingly, the boundary is described as a parametric cubic spline which provides an accurate, smooth representation with the derivatives, and hence normal, readily available. The direction of the parameter of representation is such that the fluid phase falls on the left and the solid phase on the right of the boundary as the parameter of representation increases. This allows the phase to be determined based on the direction of the normal from the boundary. This information is then used to identify points conforming to the criterion of a forcing point: being in the solid phase and having a neighbour in the fluid phase.

Application of Boundary Conditions

The calculation and application of the boundary conditions is dependent on the numerical method used to solve the governing equations of the fluid. The governing equations pertaining to this paper are,

$$\frac{\partial u_i}{\partial t} + u_j \frac{\partial u_i}{\partial x_j} = -\frac{1}{\rho}\frac{\partial p}{\partial x_i} + \nu \frac{\partial^2 u_i}{\partial {x_j}^2} + \hat{f}_{IB,i}, \tag{1a}$$

$$\frac{\partial u_i}{\partial x_i} = 0, \tag{1b}$$

where u is the velocity field in the i orthogonal direction, p represents the pressure, t the time, x a spatial direction, ρ the density, ν the kinematic viscosity and f_{IB} the forcing term relating to the imposition of the immersed boundary.

Here we consider the logic behind the immersed boundary method independently of the numerical scheme employed. Ultimately, the forcing function should equate to,

$$\hat{f}_{IB,i} = \frac{V_{\Psi,i}^{n+1} - u_i}{\Delta t} - H, \tag{2}$$

where n is the time step (the time instance for u on the RHS has been intentionally omitted as it is dependent on the selected numerical fluid solver scheme while the purpose of this equation is to elucidate the concepts of this immersed boundary technique), V_ψ is the velocity on the immersed boundary which we are attempting to impose on the fluid and H contains the convective and viscous terms of the Navier-Stokes equations. When substituted back into equation (1), hypothetically discretized by the same methodology as equation (2), the algorithm should give,

$$\frac{u_i^{n+1} - u_i}{\Delta t} = \frac{V_{\Psi,i}^{n+1} - u_i}{\Delta t}$$
$$u_i^{n+1} = V_{\Psi,i}^{n+1}. \tag{3}$$

This relation, for the rare case where the boundary lies on a computational node, states that the velocity of this node should be equal to the boundary condition imposed by the immersed boundary. In other words, if the boundary and forcing point coincide, the forcing term should act to negate the effects of surrounding fluid and directly enforce the velocity boundary condition. For the case where the points do not coincide, it is necessary to replace V_ψ with an interpolated value using the velocity on the immersed boundary and the properties of the free stream in the vicinity of the forcing point. The methodology for this interpolation will be discussed in the next subsection.

The time integration scheme used by the present solver was described in Karniadakis *et al.* (1991), and uses a splitting scheme which divides the computation of the Navier-Stokes equations into three individual operations: the explicit treatment of the non-linear terms and implicit treatment of the pressure and linear operators, respectively. These steps are

$$\frac{\hat{\mathbf{u}} - \sum_{q=0}^{J-1} \alpha_q \mathbf{u}^{n-q}}{\Delta t} = \sum_{q=0}^{J-1} \beta_q \mathbf{N}\left(\mathbf{u}^{n-q}\right), \tag{4a}$$

$$\frac{\hat{\hat{\mathbf{u}}} - \hat{\mathbf{u}}}{\Delta t} = -\nabla P^{n+1}, \tag{4b}$$

$$\frac{\gamma \mathbf{u}^{n+1} - \hat{\hat{\mathbf{u}}}}{\Delta t} = \nu \nabla^2 \left(\mathbf{u}^{n+1}\right), \tag{4c}$$

where $\hat{\mathbf{u}}$ and $\hat{\hat{\mathbf{u}}}$ are intermediate velocity fields, α, β and γ are coefficients used for the third-order (J = 3) backwards multistep method and the non-linear operator, **N**, is,

$$\mathbf{N}(\mathbf{u}) = -u_j \frac{\partial u_i}{\partial x_j}. \tag{5}$$

The presence of the immersed boundary condition is enforced in two locations. The first is in the $\mathbf{u}^n$ velocity field in the RHS of equation (4a). This is done in order to promote the presence of the immersed boundary velocity conditions in the velocity gradients of the advection step, as this is calculated explicitly, independently, and before the LHS. The second enforcement is applied through the application of equation (2) to acquire a forcing term which can be computed as,

$$\hat{f}_{IB,i} = \frac{V_{\Psi,i}^{n+1} - \sum_{q=0}^{J-1} \alpha_q \mathbf{u}^{n-q}}{\Delta t} - \sum_{q=0}^{J-1} \beta_q \mathbf{N}\left(\mathbf{u}^{n-q}\right), \qquad (6)$$

which results in the velocity field conforming to the expected immersed boundary condition at the end of this stage. Unfortunately, due to the implicit nature of the following two sub stages, incorporating the immersed boundary conditions into these steps is a non-trivial task and has not been implemented as of this paper. It is believed that this affects the effectiveness of the immersed boundary technique as the corrected values after the first stage are altered by the subsequent operations and not corrected for the immersed boundary condition. This effect contributes to the permeable boundary phenomenon reported in the following test cases.

Interpolation Technique

The interpolation method used to calculate the enforced velocity at the forcing point has been adapted from the method described in Balaras (2004). This method requires a point on the immersed boundary which possesses a normal that passes through the forcing point to be identified for every forcing point. It is along this normal that the interpolation between the immersed boundary velocity and the freestream field is conducted. The current stencil used to specify the velocity condition to be imposed on the forcing point is,

$$u^* = \begin{cases} u_{BC}, \text{ when } h_2 \text{ is very small;} \\ \dfrac{1}{1 - \dfrac{h_2}{h_1 + h_2}} \left(V_\Psi - \dfrac{h_2}{h_1 + h_2} u_{virt} \right), \text{otherwise,} \end{cases} \qquad (7)$$

where u^* is the velocity to be enforced at the forcing point, u_{virt} is the velocity interpolated at a point in the freestream specified by the lengths, h_1 and h_2, as shown in Figure 1.

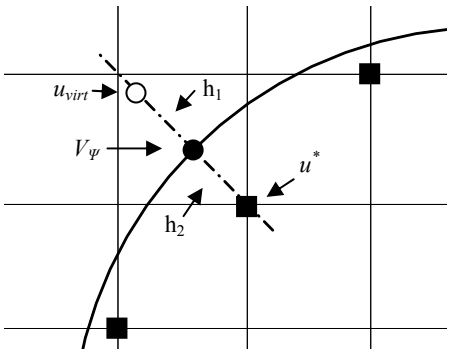

Figure 1: Schematic of the interpolation stencil being employed; h_1 and h_2 are lengths; black square - forcing points; black circle – boundary condition to be met; and white circle – virtual point.

Technique Validation

Flow Characteristics

The modelling of a stationary cylinder in uniform cross flow was conducted to determine the validity of the immersed boundary method. The nature of the wake depends heavily on the Reynolds number of the flow, providing the opportunity to assess steady state and time dependent flows by adjusting the Reynolds number. The Reynolds number was defined as,

$$Re = \frac{UD}{\nu}, \qquad (8)$$

where U is the freestream velocity, D is the diameter of the cylinder and ν is the kinematic viscosity. For these simulations velocity and length quantities were normalized allowing 1/ν to equate *Re*.

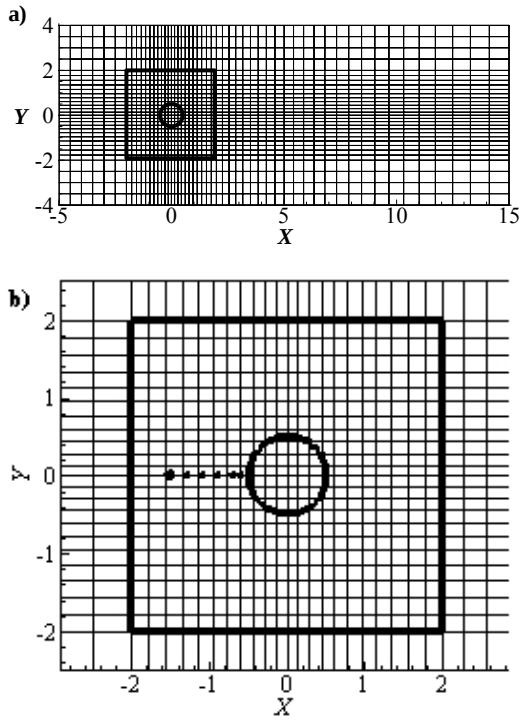

Figure 2: Schematic of validation scenario. The spectral element layout for **a)** the entire computational domain; **b)** detail in the finely resolved working area. The bounding box indicates the finely resolved working area containing the circular immersed boundary. The additional points indicate where the velocity was monitored for the validation test cases.

A schematic of the numerical setup is shown in Figure 2. Tests were conducted for Re = 25 and 30 for the steady state cases and Re = 100, 125, 150, 175 and 200 for the unsteady cases. For all cases, flows were obtained using an arbitrary Cartesian mesh combined with the immersed boundary technique as well as a boundary-conforming, body fitted mesh for comparison. The two computational domains were designed to possess a similar element count surrounding the cylinder, with approximately 480 elements located in the finely resolved working area where the cylinder resided for both cases. Figure 2 depicts the computational mesh used for the immersed boundary case.

The validity of the solutions were assessed through the comparison of the flow fields of the two solution sets at various locations, as indicated on the schematic in Figure 2b. The u-velocity was measured along the centreline approaching the leading edge and the percent difference collated. Comparisons of important characteristics of the steady and unsteady flows were also conducted.

At low Reynolds numbers, $4.5 \leq Re \leq 35$, experiments demonstrated an attached, steady, symmetric, recirculation bubble downstream of the cylinder (Coutanceau and Defaye, 1991). This characteristic was assessed as the distance from the trailing edge where the velocity in the horizontal direction, behind the cylinder and along the

centre line changed direction due to recirculation (indicating a saddle point).
Increasing the Reynolds number beyond approximately 47 results in a time dependent wake containing a Kármán vortex street (Norberg, 1994). This characteristic can be quantified by the Strouhal number,

$$St = \frac{fU}{D} = f = \frac{1}{T}, \quad (9)$$

where f is the frequency of the vortex shedding, U is the freestream velocity and D is a functional length, in this case the diameter of the cylinder. As the velocity and length quantities were normalized, this relationship can be simplified as shown where T is the period of the shedding. The Strouhal number was computed by monitoring the direction of the vertical velocity at a point 4D behind the trailing edge of the cylinder and measuring the shedding period as the time between successive cycles in direction.

RESULTS

Grid Independence Study

The time dependent case of Re = 200 was considered for both the immersed boundary and body fitted grid independence studies. This value was chosen as it was the highest Reynolds number studied in this paper and the results of any lower studies are believed to be inherently represented by these results. The nodes per element, N, were varied between 7 and 10 and the respective Strouhal numbers were computed. The percentage error between the Strouhal numbers computed for the cases where N = 7-9 and the finest case considered here, N = 10. The results indicate convergence as there is consistent agreement below the order of 10^{-2}. Ultimately, 8 nodes per element were used in the subsequent analysis, as this was considered a good intermediate value.

Flow Characteristics

Steady Flow

Figure 3 depicts a representative comparison of the pressure contour plots for the steady state cases. In particular, these plots show that the technique produces mostly smoothly varying pressure fields which display good agreement to the fields generated by the body fitted method.

A more rigorous analysis of the algorithm was conducted by considering the recirculation lengths, shown in Table 1. These values show good agreement with only a 4.30% and 3.72% difference for the Re = 25 and Re = 30 cases respectively. In comparison to values from literature, both simulations have an error of approximately 8.8%. This error is associated with the geometry of the computational domain as the distance between the upper and lower boundaries and the cylinder is small enough to significantly influence the wake (Ryan, 2004). This idea is discussed later in the unsteady results and should not be considered a detracting finding as the immersed boundary has shown very good agreement with the body fitted technique under the same computational conditions.

In order to assess the enforcement of the immersed boundary when subjected to oncoming flow, the percentage difference of the velocity approaching the leading edge between the immersed scheme and the fitted case were computed. The results are tabulated in Table 2 which shows good agreement when beyond 0.4D from the leading edge. At 0.2D the percentage difference increases from below 2% (at the points 0.4D and beyond) to between 10 -12.5%. The percentage difference then decreases at 0.1D from the leading edge. The difference at both of these locations displays a clear dependence on Reynolds number, with the point closer to the boundary showing a significantly stronger relationship to Reynolds number, decreasing from 11.31% for Re = 25 to 2.90% for Re = 200, as opposed to the slight reduction, from 12.45% to 9.88%, at the point 0.2D from the leading edge. These results show that there is slight deficiency in the enforcement of the immersed boundary.

While the method does a good job of representing the boundary overall, close to the leading, trailing, upper and lower extremes of the cylinder, it is apparent that pressure does not behave in a physical manner, as illustrated in Figure 4, where the jagged pressure contours indicate a resolution problem. As these anomalies occur in the regions of large gradient change around the boundary, it is likely that these are artefacts generated by polynomial wiggle caused by the local adjustment of the velocity by the immersed boundary forcing term. This hypothesis is supported by the fact the anomalies are contained within the elements which the boundary passes through.

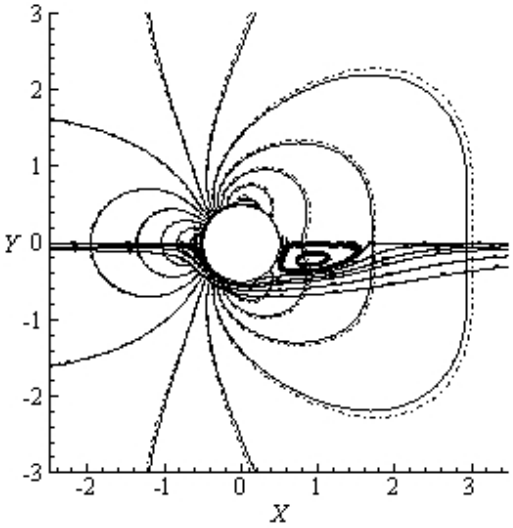

Figure 3: Typical pressure contour plot for steady state solutions where the solid contour depicts the immersed boundary case and the dashed contour the boundary conforming method. The streamlines (arrowed solid line) depict the lower half of the symmetrical recirculation region produced by the immersed boundary technique.

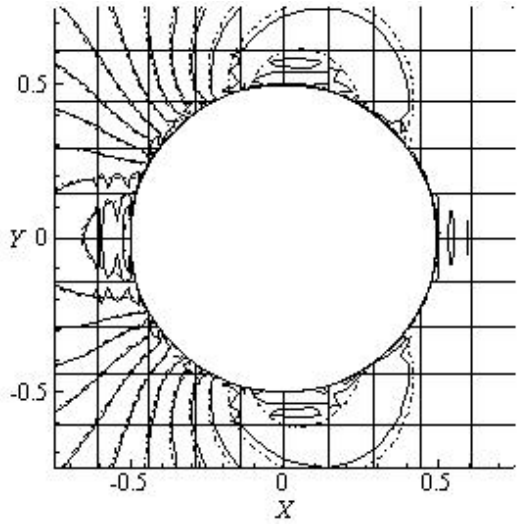

Figure 4: Closer look at the behaviour of the pressure at the boundaries for the same case as Figure 3, with the distribution of the spectral elements overlayed.

	***Re* = 25**	***Re* = 30**
Immersed Boundary	1.11	1.40
Body Fitted	1.16	1.45
% Difference	-4.30	-3.72
Coutanceau and Bouard (1977)[a]	1.22	1.53
% Difference	-8.85	-8.66

a - experimental

Table 1: Length of the recirculation bubble, measured from the trailing edge, including computed percentage differences between the various cases and the immersed boundary results.

	Re						
Position	25	30	100	125	150	175	200
0.1*D*	11.31	10.10	5.07	4.35	3.81	3.31	2.90
0.2*D*	12.45	11.84	9.56	9.52	9.62	9.74	9.88
0.4*D*	-0.11	-0.15	-0.12	-0.09	-0.05	-0.04	-0.01
0.6*D*	1.81	1.71	1.40	1.38	1.37	1.35	1.35
0.8*D*	0.91	0.86	0.73	0.73	0.75	0.77	0.81
1.0*D*	0.76	0.72	0.60	0.59	0.59	0.58	0.59

Table 2: Percentage difference of *u*-velocity along the centreline at various distances before the leading edge, over a range of Reynolds numbers.

Unsteady Flow

A representative flow for the time dependent cases is shown in Figure 5, depicting the vorticity for the case of *Re* = 200. The time-dependent cases of *Re* = 100, 125, 150, 175 and 200 showed good agreement when compared to the body fitted simulations.

The Strouhal number results are shown in Table 3. From this data, it can be seen that there is a good correlation between the two simulation techniques with the difference of the two ranging between 1.049% and 2.117%.

For comparison, the Strouhal numbers at the corresponding Reynolds numbers were predicted using Equation 10, an empirical relationship relating *Re* and *St*, (Williamson, 1988) which shows a good correlation to experimental data for parallel vortex shedding. This relationship can be expressed as,

$$St = \frac{-3.326}{\mathrm{Re}} + 0.1816 + 1.6\times10^{-4}\,Re. \qquad (10)$$

The values obtained using this relationship are tabulated in Table 3. The percentage error between these values and the reference case of the boundary conforming scheme ranged between 12.13% and 7.45%. These differences were significantly higher than the error between the two simulation methods. This disparity is due to the computational domain introducing a blockage effect caused by the proximity of the upper and lower boundaries of the domain to the cylinder. This effect was reported by Ryan (2004) where it was observed that the domain influenced the wake of a flow at *Re* = 200 by 9.7% for a domain with the upper and lower boundaries located 4*D* from the centre of the cylinder, which is also the case in this paper. The current domain was selected for efficiency and it should be noted that the most definitive results for this technique arise from the comparisons the body fitted technique, which has been proven to be very accurate (Sheard *et al*., 2007).

The jagged pressure contours observed in the stationary cases were also present in these cases (not shown here as they are of the same nature as Figure 4) although, as before, they were contained within the elements through which the boundary passed. In addition to the jagged pressure contours, the contour plots of vorticity for the unsteady cases, Figure 6, displayed significant amounts of noise at the leading edge and at an angle of approximately $\pm45^{o}$ from the trailing edge. These anomalies were not present in the body fitted cases. The oscillatory behaviour of the error at the leading edge suggests that, as with the pressure error, this is probably the result of polynomial wiggle within the element due to the adjustment of the velocity. The error towards the trailing edge is typified by the vorticity emanating from discrete points on the mesh (element nodes). A potential remedy to this currently being investigated is to increase the density of forcing points around the boundary by enforcing the boundary on both sides of the interface. This would lead to the majority of the nodes surrounding the boundary being influenced directly by a forcing node.

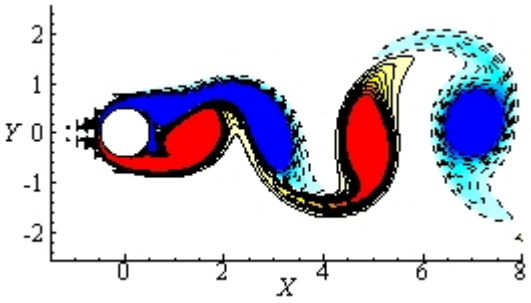

Figure 5: Contour plot of vorticity at *Re* = 200. Solid lines and red flooding - positive (anticlockwise) vorticity; dashed lines and blue flooding – negative (clockwise) vorticity.

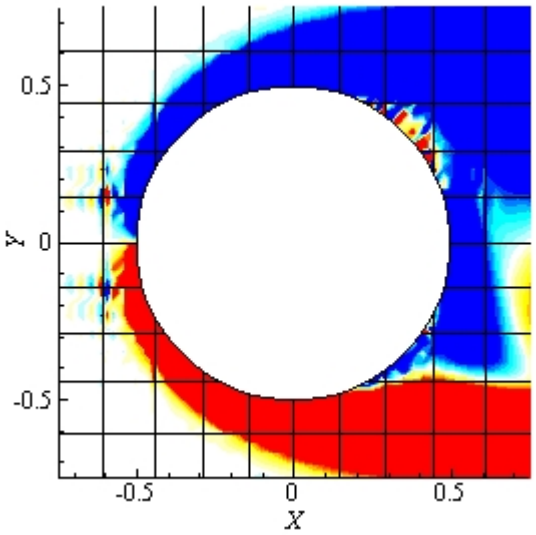

Figure 6: Erroneous regions of vorticity at the leading edge and at an angle of ±45° from the trailing edge.

	Re				
	100	125	150	175	200
Immersed	0.1858	0.1962	0.2042	0.2107	0.2162
Body Fitted	0.1839	0.1937	0.2010	0.2068	0.2117
% Diff	1.049	1.288	1.580	1.851	2.117
Williamson (1988)	0.164	0.174	0.183	0.191	0.197
% Error to Body Fitted	12.13	11.32	9.85	8.29	7.45
Ryan (2004)	-	-	-	-	0.2154
% Error to Body Fitted	-	-	-	-	-1.733

Table 3: Comparison of the recorded Strouhal number over a range of Reynolds numbers.

Boundary Permeability

Permeability of the immersed boundary was quantified by interpolating the velocity normal to the boundary at the point where V_ψ should be imposed, as shown in Figure 1. Table 4 tabulates the average absolute velocity normal to the surface (averaged by the number of forcing nodes used to represent the boundary), the number of forcing points used to represent the boundary and the maximum flux and its location for the cases of $Re = 200$ and $N = 7$-10. Overall, the average normal velocity was low, between 1.5% and 1.9% of the freestream velocity.

N	Ave Normal Velocity	Forcing Pt Count	Max Normal Velocity	Max Co-ords	
				x	y
7	0.017	116	0.111	-0.474	-0.159
8	0.018	144	0.119	-0.475	0.157
9	0.019	157	0.139	-0.494	0.074
10	0.015	184	0.133	-0.484	0.127

Table 4: Comparison of boundary permeability for the case of $Re = 200$, with various nodes per element.

The inconsistency of the results, typified by the increase in average normal velocity between $N = 7$-9 followed by the subsequent decrease at $N = 10$ and a similar trend for the maximum normal velocity, suggest that the velocity normal to the boundary is not simply a function of grid resolution. The similarity in the location of the maximum normal velocity suggests that, in addition to occurring near regions of large gradients (all appear at a slight angle to the leading edge) it is likely the geometrical layout of boundary in relation to the mesh plays a significant role in determining the velocity through the boundary. In particular, the distance between the forcing node and the boundary (h_2 in Figure 1) and the proximity of the boundary to an element edge appear to be the dominant factors in this erroneous phenomenon in the flow. The former cause relates to the accuracy of the interpolation method, while the later is due to the increasing stiffness of the Gaussian discretization as the immersed boundary approaches an element boundary. These sources of error are in addition to the diffusive action the pressure and final advection stages had on the flow solutions, which were not separable in this analysis.

FUTURE WORK

From this analysis it is apparent that the interpolation method and the way the velocities are adjusted within an element need to be further refined to reduce the magnitude of the artefacts introduced by these processes. These refinements will take the form of manipulating additional nodes within solid phase to reduce the polynomial wiggle and techniques which enforce the immersed boundary conditions within the pressure and final advection stages of the numerical scheme.

The overall generality of this technique (no special cases) makes its adaptation to moving boundaries relatively straight forward. Furthermore, coupled with an appropriate force feed-back system, this methodology presents the opportunity for the simulation of fluid-structure interactions.

CONCLUSIONS

This study has presented the methodology for integrating an immersed boundary algorithm into a spectral element fluid solver. The preceding work has shown that the implementation of the immersed boundary technique into a spectral element fluid solver is capable of producing results which shows good agreement to a boundary conforming method for both steady and unsteady flows. The technique predicted the recirculation length behind a fixed circular cylinder in a cross flow to 4.30% and 3.72% for the steady cases of $Re = 25$ and 30 respectively when compared to the same scenario simulated using a boundary conforming method. Similarly, the prediction of the Strouhal numbers for the time-dependent cases was computed to be within 2.2% for the range of $Re = 100$ - 200. A brief analysis of the permeability of the immersed boundary demonstrated that it was quite low, on average less than 2% of the freestream velocity. Overall, this paper has shown that the immersed boundary method is compatible with spectral element fluid solvers. This technique will form the basis for future work to implement a fluid-structure interaction algorithm into this fluid solver. Ultimately, numerical simulation of fluid-structure interactions could aid in the investigation of complex industrial and medical phenomenon.

ACKNOWLEDGEMENTS

The author would like to thank the Department of Mechanical and Aerospace Engineering, Monash University for their support.

REFERENCES

BALARAS, E., (2004), "Modeling complex boundaries using external force field on fixed Cartesian grids in large-eddy simulations", *Comput. Fluids* **33**, 375-404.

COUTANCEAU, M. and BOUARD, R. (1977), "Experimental Determination of the Main Features of the Viscous Flow In the Wake Of A Circular Cylinder In Uniform Translation – 1 Steady Flow", *J. Fluid Mech.* **79(2)**, 231

COUTANCEAU, M. and DEFAYE, J. R., (1991), "Circular cylinder wake configurations. a flow visualization survey" *Appl. Mech. Rev.* **44**, 255.

KARNIADAKIS , G. E., ISRAELI, M., and ORSZAG, S. A., (1991), "High-order splitting methods for the incompressible Navier-Stokes equations," *J. Comput. Phys.,* **97**, 414-443

KIM, J., KIM, D. and CHOI, H., (2001), "An immersed-boundary finite-volume method for simulations of flow in complex geometries", *J. Comput. Phys.,* **171**, 132-150

NEWMAN, D.J. and KARNIADAKIS, G.E., (1997), "A direct numerical simulation study of flow past a freely vibrating cable", *J. Fluid Mech.,* **344**, 95–136.

RYAN, K., (2004), "The Analysis of Wake Structures Behind Stationary, Freely Oscillating and Tethered Cylinders", *PhD Thesis, Department of Mechanical and Aerospace Engineering, Monash University*

SHEARD, G.J., LEWEKE, T., THOMPSON, M.C. & HOURIGAN, K. (2007), "Flow around an impulsively arrested circular cylinder", *Phys. Fluids* **19**(8), article number 083601

WILLIAMSON, C.H.K., (1988), "Defining a universal and continuous Strouhal-Reynolds number relationship for the laminar vortex shedding of a circular-cylinder", *Phys. Fluids* **31**, 2742-2744

YANG, J., PREIDIKMAN, S. and BALARAS, E., (2008), "A strongly coupled, embedded-boundary method for fluid–structure interactions of elastically mounted rigid bodies"*, J. Fluids Struct.* **24** 167–182.

